



This is a repository copy of *Lubrication of a flexible piston skirt conjunction subjected to thermo-elastic deformation: A combined numerical and experimental investigation.*

White Rose Research Online URL for this paper:  
<http://eprints.whiterose.ac.uk/94605/>

Version: Accepted Version

---

**Article:**

Littlefair, B., De La Cruz, M., Mills, R. et al. (4 more authors) (2014) Lubrication of a flexible piston skirt conjunction subjected to thermo-elastic deformation: A combined numerical and experimental investigation. *Proceedings of the Institution of Mechanical Engineers, Part J: Journal of Engineering Tribology*, 228 (1). pp. 69-81. ISSN 1350-6501

<https://doi.org/10.1177/1350650113499555>

---

**Reuse**

Unless indicated otherwise, fulltext items are protected by copyright with all rights reserved. The copyright exception in section 29 of the Copyright, Designs and Patents Act 1988 allows the making of a single copy solely for the purpose of non-commercial research or private study within the limits of fair dealing. The publisher or other rights-holder may allow further reproduction and re-use of this version - refer to the White Rose Research Online record for this item. Where records identify the publisher as the copyright holder, users can verify any specific terms of use on the publisher's website.

**Takedown**

If you consider content in White Rose Research Online to be in breach of UK law, please notify us by emailing [eprints@whiterose.ac.uk](mailto:eprints@whiterose.ac.uk) including the URL of the record and the reason for the withdrawal request.



[eprints@whiterose.ac.uk](mailto:eprints@whiterose.ac.uk)  
<https://eprints.whiterose.ac.uk/>

# Lubrication of a flexible piston skirt conjunction subjected to thermo-elastic deformation: a combined numerical and experimental investigation

B.Littlefair<sup>1)</sup>, M. De La Cruz<sup>1)</sup>, R. Mills<sup>2)</sup>, S. Theodossiades<sup>1)</sup>, H.Rahnejat<sup>1)</sup>\*, R. Dwyer-Joyce<sup>2)</sup>, S. Howell-Smith<sup>3)</sup>

<sup>1)</sup> Wolfson School of Mechanical & Manufacturing Engineering

Loughborough University, Loughborough, UK

<sup>2)</sup> The Leonardo Centre for Tribology, University of Sheffield, Sheffield, UK

<sup>3)</sup> Capricorn Automotive, Basingstoke, Hampshire, UK

\*Corresponding author: [H.Rahnejat@lboro.ac.uk](mailto:H.Rahnejat@lboro.ac.uk)

## Abstract

*The piston-cylinder conjunction accounts for nearly 50% of all the parasitic frictional losses in an IC engine of which the piston skirt accounts for nearly half of these losses. Consequently, part - circumferential short skirted compliant pistons have become a development trend, particularly for high performance engines. Another trend has been the use of light weight moving parts to reduce inertial imbalance. This has led to the use of shorter lighter pistons constructed from lower density materials, such as aluminium. These higher power density pistons typically operate at elevated temperatures and undergo significant mechanical and thermal distortions due to the relatively high thermal expansion coefficients. As a result thermo-mechanical distortion of the skirt plays an important role in controlling the clearance gap between the skirt and the liner and makes the analysis, particularly skirt deformation a computationally intensive procedure. The paper presents a semi-automatic methodology for the prediction of piston skirt thermo-mechanical deflection, which incorporates skirt deformation as well as piston crown compliant contribution to the skirt-liner clearance. This procedure is based on the creation of a compliance matrix and its intricate manipulation, significantly reducing the simulation run times. Integration of this approach with the numerical solution of Reynolds equation leads to an accurate prediction of film thickness. In addition, an array of ultrasonic sensors is used to directly measure the conjunctional lubricant film thickness in a non-invasive manner. The predictions and measurements show good conformance, an approach not hitherto reported in literature.*

**Keywords:** IC engines, piston skirt, thermo-mechanical distortion, film thickness measurement

## 1. Introduction

Frictional losses in the piston skirt-to-cylinder liner conjunction account for approximately 3% of the input fuel energy according to Fitzsimons [1], who also states that piston ring pack losses account for a further 4% of the fuel energy. All these losses are primarily composed of viscous shear of the lubricant film and asperity interactions of the contiguous surfaces. However, for most of the piston cycle the regime of lubrication in the skirt-liner conjunction is dominated by hydrodynamic or soft elastohydrodynamic (iso-viscous elastic) regimes of lubrication [2,3]. Therefore, aside from piston reversals at the dead centres, where mixed regime of lubrication can ensue, friction is usually generated through viscous shear of a lubricant film. Consequently, it has been surmised that reducing the lubricant viscosity would improve engine efficiency. However, the limiting factor is the lubricant load carrying capacity in conjunctions with relatively high load intensity, such as the cam-follower conjunction [4]. Alternatively, a smaller piston skirt area would

decrease friction and may encourage piezo-viscous action of the lubricant. This could encourage elastohydrodynamic conditions, which would yield lowest friction [5,6]. Light pistons in high performance engines employ compliant skirts due to their overriding low section stiffness in the interest of reduced overall inertia. The growing emphasis on the reduction of reciprocating mass and the increased demands brought on by downsizing has had a significant effect on the loads the piston skirt needs to support and hence the deformation and lubricated conjunctural performance. Predicting the effects of these increasing demands on the lubrication mechanism is the key to the ongoing development of high performance pistons. Perera *et al* [7] provide a basic friction model in their multi-body analysis of a single cylinder engine. However, their simple model does not provide accurate prediction of conjunctural behaviour, particularly the effect of piston skirt compliance under thermo-elastic deformation.

There have been various contributions dealing with piston flexibility both with and without lubrication models [8,9]. Often the finite element mesh density and the computational times are the concerns. Due to computational limits many techniques previously employed have been quasi-static, so that the distortions are calculated prior to the determination of generated pressures. In reality the deformed *in situ* running profile of the conjunctural bounding solids are as the result of the generated pressures. Thus, the calculation of conjunctural geometry should be updated within a spatial domain iteration process. This approach was employed by Balakrishnan *et al* [3, 10] for both transient and quasi-static lubrication studies, but the deformation of the bounding solids was confined to the localised contact domain, treating them as semi-infinite elastic solids. The global thermo-elastic deformation of the contacting solid surfaces was ignored.

The importance of piston skirt shape is well understood and the features are *optimized* to account for the differential thermal expansion, whilst still offering adequate entraining geometries. The in-service shape is much harder to control as this is the result of various mechanical distortions. Recently, Hoshikawa *et al* [11] showed, through experimental techniques, the effect of stiffness modification and compared it with observation of frictional changes using a floating liner set up. Qualitative observations from a visual liner were also made. Bai [12] also showed the effect of modifying the structural stiffness of the skirt using techniques detailed earlier by McClure [13]. The effect of piston structural stiffness on contact condition, film shape and generated pressures were discussed [14]. Partial verification was reported through LIF (laser induced fluorescence) observation of the contact, which gave a rough qualitative comparison in terms of clearance and film shape. A single point measurement comparison on a *cold* profile has been reported by Dwyer-Joyce [16].

In this paper a high performance, single cylinder spark ignition engine is used with film thickness measurement carried out by ultrasonic sensors adhered to the outside wall of the liner, on the thrust side. Furthermore, numerical predictions are carried out through combined solution of Reynolds equation for piston skirt-liner contact with the conjunctural elastic film shape, which incorporates the thermo-elastic distortion of a structurally flexible piston. Using the measured engine boundary conditions with the numerical method allows for a specific solution to be generated. The resulting predicted film thickness is compared with that measured by the ultrasonic sensors. The technique for the calculation of distortion is further developed allowing for significantly decreased computation times without foregoing accuracy or precision. The high speed measurement of film thickness is carried out for the direct validation of numerical predictions.

## 2. Experimental methodology

### 2.1. Experimental Boundary conditions

A Honda CRF 450R single cylinder 4-stroke engine is used throughout the investigations as a base for the measurements and for the predictive analysis. A Leine and Linde optical encoder is positioned on the engine crankshaft, allowing for crank angle-based data acquisition. Amongst other parameters, engine speed, in-cylinder pressure and film thickness are recorded throughout engine testing. The engine is resisted by an Oswald 250 kW transient dynamometer and controlled to a nominal speed of 4250 rpm. Single cylinder engines are inherently unbalanced with a plethora of engine order vibration [15]. Taking this fact into account, the engine speed is regarded as an average of its whole cycle, whose variance is captured and shown in Figure 1. Steady state thermal condition is controlled at 70°C water coolant temperature and 104°C bulk oil temperature. For these steady state tests the temperature of the cylinder liner wall is monitored by embedded thermocouples into the liner wall, 0.8mm from the conjunctural surface. The average of the temperature readings is used as the starting point for the temperature of the contact lubricant in both numerical analysis, as well as calculation of the acoustic properties of the lubricant, necessary for use in the ultrasonic measurements.

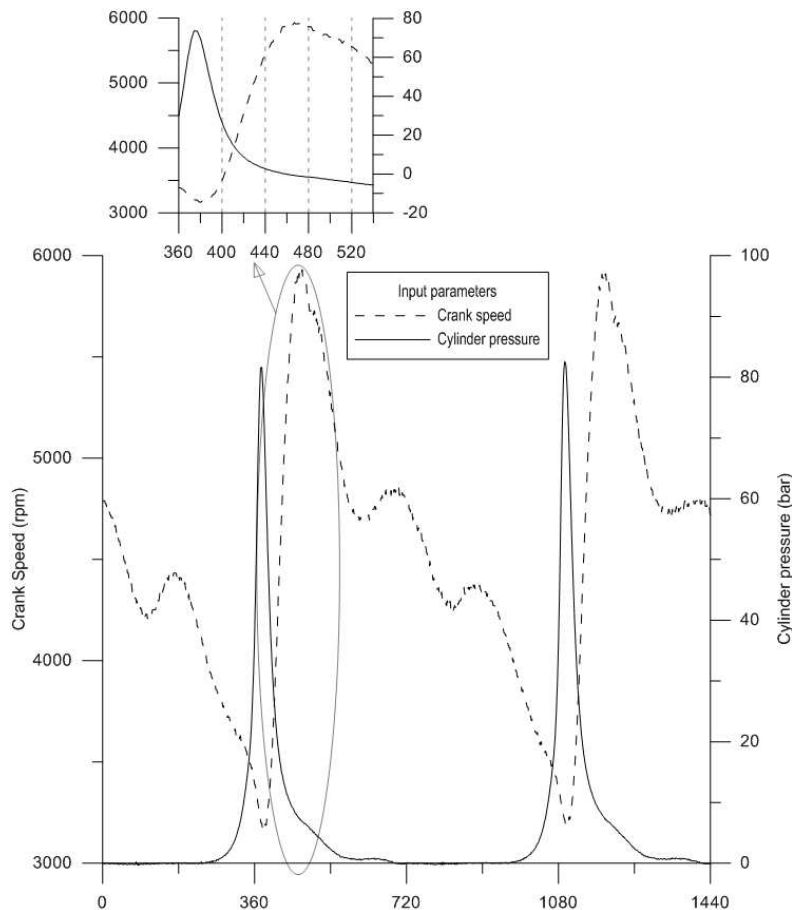
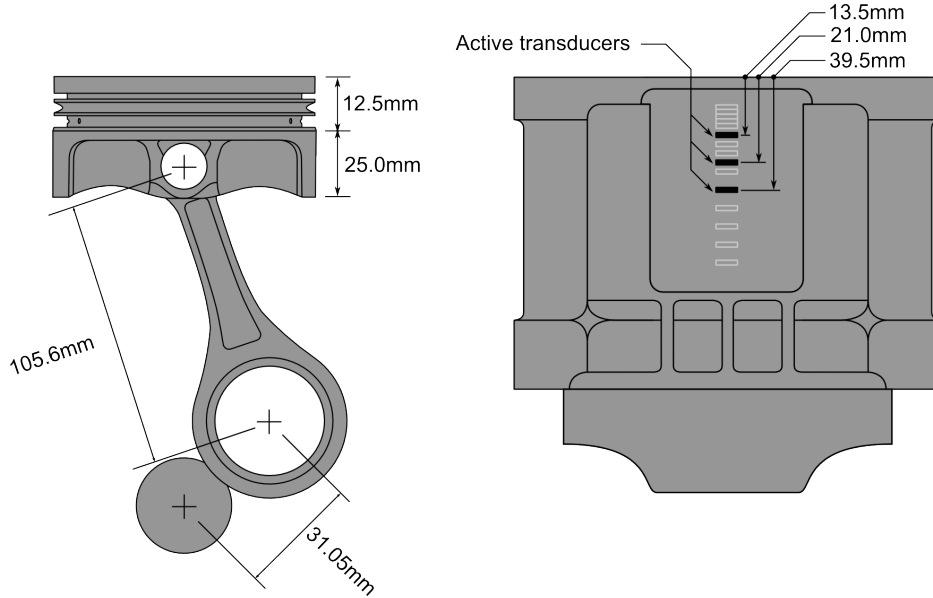


Figure 1: Variation of gas pressure and engine speed for two typical cycles

### 2.2. Film thickness measurement

A series of ultrasonic transducers (5mm x 1mm) were appropriately sealed and positioned axially along the exterior surface of the cylinder liner (within the water jacket) (figure 2) [16]. They were used to measure the instantaneous film

thickness at the thrusting skirt-cylinder interface. These transducers generated ultrasonic pulses, which travelled through the cylinder wall and were reflected from the interface. The reflected pulses were captured and amplified, and the reflection coefficient was obtained for the 10MHz central frequency of the transducers (as outlined by Avan *et al* [17] and Mills *et al* [18]).



**Figure 2: Schematics showing position of sensors on cylinder liner exterior wall**

Using equation (1) the film thickness was calculated, where  $\rho$  is the lubricant density,  $c_s$  is the speed of sound in the lubricant,  $Z$  is the acoustic impedance of the skirt and cylinder materials (both made of hyper-eutectic aluminium) and  $|R|$  the reflection coefficient magnitude of the 10MHz component:

$$h = \frac{2\rho c_s^2}{\omega Z} \sqrt{\frac{|R|^2}{1-|R|^2}} \quad (1)$$

The data acquisition rate was set at 80k/s. The duration of each measurement was 350 ns, corresponding to a piston translation of  $1.5\mu\text{m}$  at approximately  $20^\circ$  ATDC (after top dead centre), therefore, it may be regarded as almost instantaneous. The crank angle was simultaneously recorded for each ultrasonic pulse, allowing the skirt position to be determined. During a test run, measurements were acquired sequentially for each sensor for a period of 2 seconds. Therefore, the results presented correspond to the mean lubricant film thickness profile obtained from approximately 100 engine cycles.

### 3. Numerical analysis

#### 3.1. Loading and contact kinematics

A number of parameters need to be determined as input data for numerical predictions. The net side force (contact force) can be calculated from the primary applied forces and the instantaneous connecting rod angle [6] as:

$$F_s = \left( (P_c \pi r_p^2) + (m_g + m_p) \frac{dy_p}{dt} \right) \tan \phi \quad (2)$$

The engine design incorporates a crank offset of 7.5 mm. This arrangement increases the engine's transmitted torque during combustion and reduces the side loading compared with a conventional centralised crank [19].

The instantaneous connecting rod angle,  $\phi$  is obtained as:

$$l \sin \phi = C_p + r \sin \theta \quad (3)$$

The piston speed is calculated using the instantaneous measured crank speed as:

$$\frac{dy_p}{dt} = \frac{dy_p}{d\theta} \frac{d\theta}{dt} \cong r\omega \left( \sin \theta + \frac{\Lambda}{2} \sin 2\theta \right) \quad (4)$$

where:  $\Lambda = \frac{r}{l}$ ,

The resulting side force (ignoring rod inertial contribution and the small end torque effects of the gudgeon pin within the bearing surfaces of the piston and connecting-rod) and piston speed are shown in Figure 3, this is based on the input data shown in Figure 1.

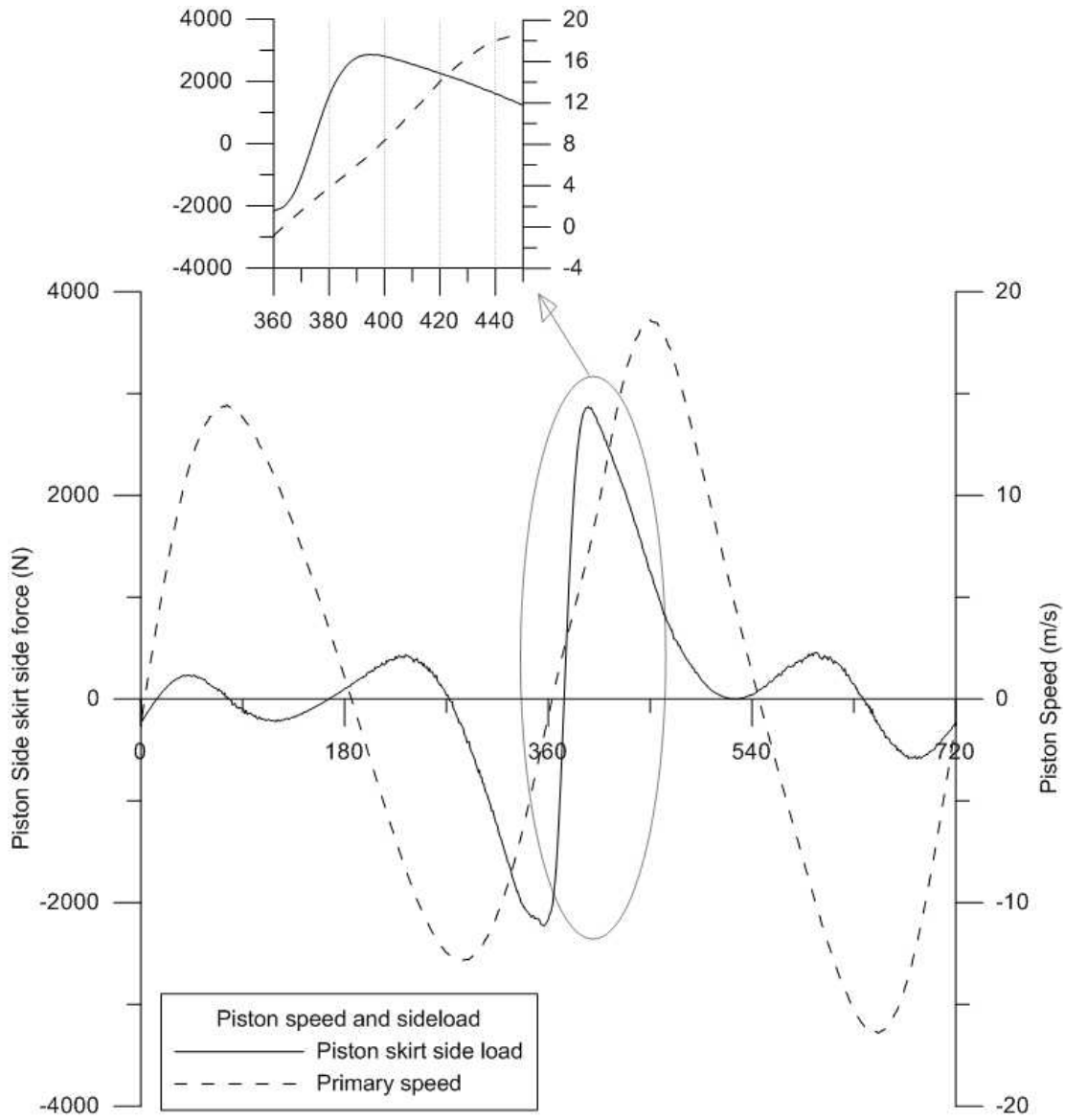


Figure 3: Side force and piston speed for a given cycle

### 3.2. Numerical model

The prediction of tribological conditions in the piston skirt-cylinder liner conjunction is achieved through combined solution of the instantaneous elastic film shape (including the thermo-mechanical distortion) and Reynolds' equation (also accounting for the load carried by counterface asperities).

#### 3.2.1 Hydrodynamics

The general form of Reynolds equation is:

$$\frac{\partial}{\partial y} \left[ \frac{\rho h^3}{\eta} \frac{\partial p}{\partial y} \right] + \frac{\partial}{\partial z} \left[ \frac{\rho h^3}{\eta} \frac{\partial p}{\partial z} \right] = 12 \left\{ u_{av} \frac{\partial}{\partial y} (\rho h) + v_{av} \frac{\partial}{\partial z} (\rho h) + \frac{d}{dt} (\rho h) \right\} \quad (5)$$

The ultimate term on the right-hand side of the equation is due to squeeze film motion, which has its most significant

contribution in a transient analysis and at the dead centre piston reversals where there is momentary cessation of contribution at low entraining motion [3]. The most important positions for the analysis of thermo-elastic deformation of piston skirt and its effect upon lubrication are during the combustion stroke with significant contact load and chamber temperature. For the position reported in the current analysis, there is a contact force of 2091N and the piston sliding speed of 4.4 m/s, the latter ensuring the dominance of Couette entrainment flow (first term on the right hand side of equation (5)). The speed of entraining motion,  $u_{av}$  is given by:

$$u_{av} = \frac{1}{2} \frac{dy_p}{dt} = \frac{y_p}{2} \quad (6)$$

Furthermore, it is assumed that there is negligible side leakage flow of the lubricant in the circumferential contact direction, if viewed as unwrapped;  $z_p$ . Hence, the second term on the right hand side of Reynolds equation may also be neglected.

The Reynolds equation is solved simultaneously with the elastic film shape:

$$h_{i,j} = s_{i,j} - \delta_{i,j} + c \quad (7)$$

where, the deflection at the nodal surface position,  $i,j$  is as the result of thermo-elastic deformation of the skirt induced by an assortment of loading conditions, described in section 3.3.  $c$  is the initial nominal radial clearance of 18  $\mu\text{m}$  which is altered depending on the load convergence criterion in section 3.4.

The lubricant rheology (density and viscosity) play an important role if piezo-viscous conditions are encountered. In particular, the lubricant viscosity should be adjusted for the steady-state operating temperature of the skirt-cylinder liner interface (110°C), which is derived as an average of the measured liner temperatures. The dynamic lubricant viscosity-pressure dependence is obtained as [20], where  $\eta_0$  is the effective viscosity at the inlet temperature of 110°C:

$$\bar{\eta} = \frac{\eta}{\eta_0} = \exp(\ln \eta_0 + 9.67)(-1 + (1 + 5.1 \times 10^{-9} p)) \quad (8)$$

The density variation with pressure is as proposed by Dowson and Higginson [21], again with the density  $\rho_0$  adjusted for the interface temperature:

$$\rho = \rho_0 \left( 1 + \frac{0.6 \times 10^{-9} p}{1 + 1.7 \times 10^{-9} p} \right) \quad (9)$$

### 3.2.2 Boundary contribution

The load carried by the skirt is supported by a combination of generated hydrodynamic lubricant pressures and those carried by a small proportion of surface asperities. The load carried by the asperities is calculated according to the model proposed by Greenwood and Tripp [22]:

$$W_a = \frac{8\sqrt{2}}{15} \pi (\zeta k \sigma)^2 \sqrt{\frac{\sigma}{k}} E' A_c F_{5/2}(\lambda) \quad (10)$$

The dimensionless group  $\zeta\kappa\sigma$  is known as the roughness parameter,  $\sigma$  which is the root mean square roughness of contiguous surfaces and  $\sigma/\kappa$  is a measure of a typical asperity slope [6]. These are obtained through topographical measurements. It should be noted that the method in [22] assumes a Gaussian distribution of surface asperities. The statistical function  $F_{5/2}(\lambda)$  is introduced to match the assumed Gaussian distribution of asperities as a function of the Stribeck oil film parameter,  $\lambda = \frac{h(x,y)}{\sigma}$  [22].

In order to make this function amenable to simple computation, two different approaches are proposed. The first is due to Hu *et al* [23], using a non-linear representation as:

$$F_{5/2}(\lambda) = \begin{cases} A_c(4-\lambda)^\beta; & \lambda \leq 4 \\ 0 & ; \lambda > 4 \end{cases} \quad (11)$$

in which  $A_c = 4.4068 \times 10^{-5}$  and  $\beta = 6.804$ . In fact, by choosing a changeover parameter of 4, Hu *et al* [23] extended the upper limit for the mixed regime of lubrication from the usual value of  $\lambda = 3$  to  $\lambda = 4$ .

The alternative relationship uses a fifth order polynomial curve fit to represent equation (10) for  $j=1$  [24]:

$$F_{5/2}(\lambda) = -0.0046\lambda^5 + 0.0574\lambda^4 - 0.2958\lambda^3 + 0.7844\lambda^2 - 1.0776\lambda + 0.6167 \text{ where; } F_{5/2}(\lambda) > 0 \quad (12)$$

The usual cross-hatch honed cylinder liners do not follow a Gaussian topographical distribution. Thus, a piston without the common tooling marks has been used in the current study to reduce the complexity of the analysis. This allows for the use of Greenwood's nominally flat contact assumption and reduces the uncertainty in the measurement of film thickness. The topographical parameters of the specifically designed and manufactured liner and skirt surface have been measured and are included with the material properties in table 1.

**Table 1 - Material and topographical parameters**

Parameter	Value	Unit
Liner Material	Aluminium AA2618	-
Modulus of elasticity of liner material	75	GPa
Poisson's ratio for liner material	0.33	-
Piston Material	AA2618 Aluminium	-
Modulus of elasticity of piston material	75	GPa
Poisson's ratio of piston material	0.33	-
Ra for liner	0.26	$\mu\text{m}$
Rk for liner	0.298	$\mu\text{m}$
Ra for Skirt	0.299	$\mu\text{m}$
Rk for Skirt	0.174	$\mu\text{m}$
Roughness parameter ( $\zeta\kappa\sigma$ )	0.138	-
Measure of asperity gradient ( $\sigma/\kappa$ )	9.8e-4	-

### 3.3. Piston body distortion

The thermo-mechanical distortion of the piston skirt is a crucial part of the tribological conditions. An adequate formulation yields numerical results which are much closer to the real *in situ* conditions. The instantaneous contact shape is a function of four main parameters. These are: (1)- mechanical distortion of skirt due to the applied reaction forces, (2)- global mechanical distortion due to the application of combustion gas pressure, (3)- distortion of piston subjected to inertial force, and (4)- global thermal distortion [14].

#### 3.3.1 Distortion due to normal skirt reaction forces, compliance method ( $\delta SI$ )

The hydrodynamic and boundary pressures, acting on the thrust and anti-thrust sides of the piston, induce a reaction force orthogonal to the skirt surface. In order to calculate the response of the skirt's surface, an FEA half-piston model is generated with planar symmetry along the X-Y plane, using Patran for the controlled meshing and imposition of appropriate constraints. The resulting model uses 10-noded tetrahedral elements for the solid geometry. In the model shown in figure 4, approximately 30,000 nodes were employed. Mirrored boundary conditions were applied on the half-model, while the pin bore nodes were fixed. The mirror boundary condition is valid for cases of symmetrical skirt loading. This assumption is only rendered invalid when non-uniform bore distortions are included, which is not addressed in the case presented here. A uniform isothermal profile is used for the liner providing constant thermal radial growth. The pin-bore constraint represents the opposing gudgeon pin and crank reactions by using a rigid constraint in all the X,Y, Z directions on the pin bore nodes.

The mesh introduced in the model has the same spacing, size and alignment as that used for the solution of Reynolds' equation, enabling a direct correspondence between the calculated pressures and the film shape. Other authors have used interpolation algorithms [13], summing the viscous and boundary pressures over large areas and only concentrating on a handful of nodes on the contacting surfaces (D'Agostino *et al* [25] and Ning *et al* [26]). This may lead to errors through interpolation; the typical shapes produced cannot be calculated accurately using basic interpolation algorithms. The crucial step is to avoid long computations in the determination of global deformation of the piston skirt.

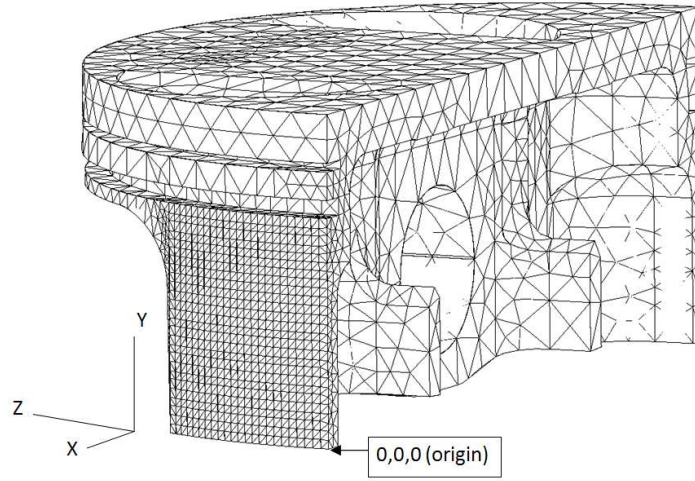


**Figure 4: Meshing of the piston skirt**

The stiffness matrix is directly exported from the FE solver (MSC Nastran R3c in this case). For the calculation of deflection equation (13) is solved using the preconditioned conjugate gradient (PCG) method [27]:

$$[F][K]^{-1} = [\delta SI] \quad (123)$$

As the lubricant pressures are updated iteratively, the solution of equation (13) dominates the computational effort required for each iteration step. To improve this, a compliance matrix is created.

For each nodal position on the skirt a unit load,  $L_u$ , is applied normal to the skirt surface and the nodal response is recorded in the  $x$  and  $z$  directions. Applying this load for each nodal position on the skirt, in isolation and sequentially, allows for a 5 dimensional reduced array to be formed,  $A(i, j, k, l, n)$ , where  $i$  and  $j$  refer to the position of the load,  $k$  and  $l$  refer to the skirt nodal position and  $n$  is either 1 or 2 for the respective  $x$  or  $z$  deflection. A special case for the edge and corner nodes has been applied, this being  $L_u/2$  and  $L_u/4$  respectively, in order to account for the reduced nodal areas.

As the deflection calculations are performed using a linear analysis, a scaled addition for each response shape to a given load type can be performed. Therefore, the effect of combined forces on the final distorted geometry can be predicted. The summation of these effects is provided by equation (14) for one of the Cartesian directions. In terms of the computational burden, the calculation for any given location/condition is 4 orders of magnitude faster than the repetitive PCG solution method. On a typical desktop machine it improves the solution time of a single load case from 30-40 seconds to 3-4 ms. This approach has been validated against the Nastran results for the same condition and for the equivalent case when the assumption of plane-symmetrical boundary conditions is relaxed.

$$[\delta_n]_{k,l} = \sum_{m_{yy}}^{i=1} \sum_{n_{zz}}^{j=1} \sum_{m_{yy}}^{k=1} \sum_{n_{zz}}^{l=1} [\delta_n]_{k,l} + \left( [A]_{i,j,k,l,n} \cdot \frac{F_{(i,j)}}{L_u} \right) \quad (134)$$

where  $F$  is given as:

$$[F] = ([P_v] + [P_b]) dz dy \quad (145)$$

### 3.3.2 Distortion due to in-cylinder pressure ( $\delta C_p$ )

It is clear that the combustion chamber pressure has a significant effect upon the instantaneous contact geometry of the skirt. Over the past few years, this has become an even greater influence due to engine downsizing, whilst maintaining or increasing the overall output (increasing specific output) in order to reduce fuel consumption, thus emissions. The effect of crown stiffness on friction and contact patch has been recently experimentally highlighted by Hoshikawa *et al* [11]. It is, therefore, very important to introduce a technique that is sensitive to the more compliant pistons and their skirts and sufficiently accurate to predict the piston skirt's load carrying capacity.

Using the same finite element model as that producing the stiffness arrays, the crown loading may be applied in a single static case for a half piston model with symmetrical boundary conditions. The constraining reaction is provided by the upper surface of the pin bore with only imposed  $y$ -direction constraint, replicating a vertical reaction from the gudgeon pin – bore interface. As this load case is treated independently and the resulting deflection is assumed to be linear, the direct proportionality between the in-cylinder pressure and the skirt deflection in the  $xz$  plane is obtained.

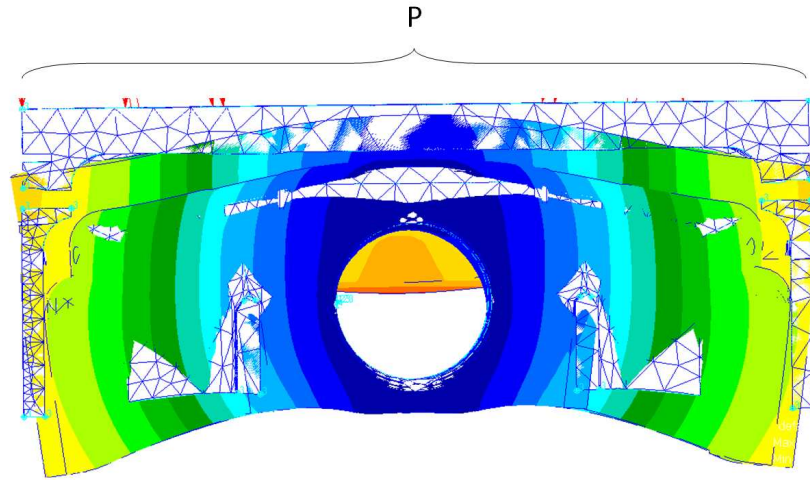


**Figure 5: Crown loading in FEA package**

The case shown in Figure 55 is for a unit combustion pressure applied to the crown top surface and shows the mode of deflection induced by crown pressure loading. The same analysis is performed for a higher pressure of 20MPa, and the same distorted shape is observed, but with different extent of deformation. As a linear analysis is performed this would be entirely expected and thus the crown deflection array ( $[\varepsilon]$  with dimensions  $n_{yy}$  and  $n_{zz}$ ), is devised and applied using equation (16). The use of the scaled solution allows for a fast calculation procedure to obtain the skirt shape change with respect to cylinder pressure rather than the repetitive solution of the linear set of stiffness equations.

$$[\delta C_p] = \frac{P_{cy}}{P_{ref}} [\varepsilon] \quad (156)$$

For this procedure to be included in the overall analysis, a skirt response shape is generated for a unit pressure loading. Using this response shape and a scaling factor for cylinder pressure ratios, a rapid solution method is devised. This analysis is based on the following assumptions / simplifications:

- The cylinder pressure acts evenly over the surface of the piston crown
- The deflection of the crown has a negligible effect upon the direction of application of pressure
- The changing connecting rod angle has no appreciable effect on the constraining direction of the gudgeon pin axis

### 3.3.3 Primary inertial deformation ( $\delta In$ )

The effect of inertial loading is very similar to that of crown loading, described above. However, in this case, the inertial force reverses direction. With the same half model, a sample of inertial load cases with given accelerations are performed using a linear solution. A shape array for the skirt is created for both the upstroke and down-stroke senses of primary acceleration (both with dimensions  $n_{yy}$  and  $n_{zz}$ ). Using these shape arrays and a given primary acceleration magnitude, the resulting skirt deformation profile can be input into the elastic film shape, using:

$$[\delta In] = \frac{\int_{ca}^{\int_p}}{\int_p} [\varepsilon ip] \text{ or } [\delta In] = \frac{\int_{ca}^{\int_m}}{\int_m} [\varepsilon in] \quad (167)$$

### 3.3.4 Thermal Distortion ( $S_{i,j}$ )

The piston structure is subjected to a large thermal gradient resulting from the combustion temperature present in the cylinder chamber during engine fired conditions. The cooling effect of the oil jet directed towards the piston crown prevents the cylinder system from thermal overload which otherwise may lead to catastrophic seizure. The 2D temperatures have been obtained on a SI engine of a similar power output running at WOT (wide open throttle) [28]. Using these as the target temperatures and altering the convective coefficients accordingly within a Nastran thermal solution, a 3D temperature profile is created [14], which enables a finite element analysis to obtain the thermal expansion of the piston relative to the uniform base *cold* geometry at ambient temperature. This single thermally expanded profile is used as the base piston skirt profile  $S_{i,j}$  in the elastic film shape (equation (7)).

The final expression for the nodal deflection,  $\delta_{i,j}$ , used in equation (7) is obtained as:

$$\delta_{i,j} = \delta Cp_{i,j} + \delta In_{i,j} + \delta Sl_{i,j} \quad (178)$$

## 3.4. Method of solution

There are two convergence criteria to be met before a final solution is obtained. First, pressure convergence is sought as:

$$\frac{\sum_{i=1}^{ny} \sum_{j=1}^{nz} |P_{(i,j)}^{it} - P_{(i,j)}^{it-1}|}{\sum_{i=1}^{ny} \sum_{j=1}^{nz} P_{(i,j)}^{it}} \leq \varepsilon_{rp} \quad (19)$$

The error tolerance  $\varepsilon_{rp}$  is set to  $10^{-4}$  [3]. If the criterion is not satisfied, then each of the nodal pressures is updated as:

$$P_{(i,j)}^{it} = P_{(i,j)}^{it-1} + \vartheta_p \Delta P_{(i,j)}^i \quad (180)$$

where  $\vartheta_p$  is a relaxation factor, typically 0.5.

Second, the load convergence criterion is:

$$|W - F_s| \leq \varepsilon_L \quad (191)$$

where  $\varepsilon_L$  is the error tolerance for load convergence (set to 0.1%), the load is given by  $F_s = \iint p \cdot dydz$

When this criterion is not met the initial assumed clearance is altered as:

$$c = c_{n-1} \left( \left( \frac{F_s}{W} \right)^\Omega \right) \quad (202)$$

$\Omega$  is the relaxation factor, typically in the order of  $10^{-5}$ .

#### 4. Results and Discussion

This initial investigation is confined to the crank angle position of 23°ATDC, at 4250 rpm with 90% throttle, and the input data from figures 1 and 3. The analysis is carried out for this position as it exhibits relatively high side load and due to the geometrical constraints restricting the placement of the ultrasonic sensors. The direct centre line comparison shows good correlation between the predictions and measurements as shown in Figure 6. Although this comparison shows a good quantitative correlation, particularly in terms of shape and minimum film thickness, it cannot confirm the full 3D predicted film thickness of the entire skirt. The solid plot in Figure 6 is the predicted film thickness profile, marked along the centre line of the oil film thickness contour of figure 7. The positions of film thickness minima are in fact to either sides of the centre line, approximately 7mm away circumferentially.

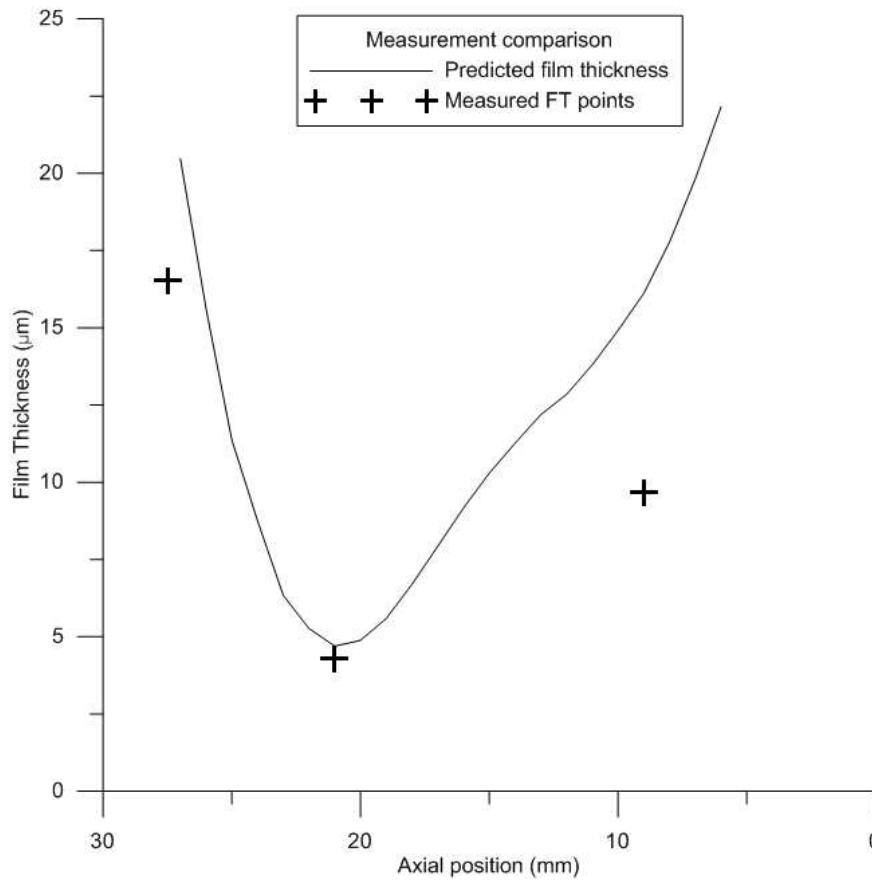


**Figure 6 - Centre line film thickness comparison**

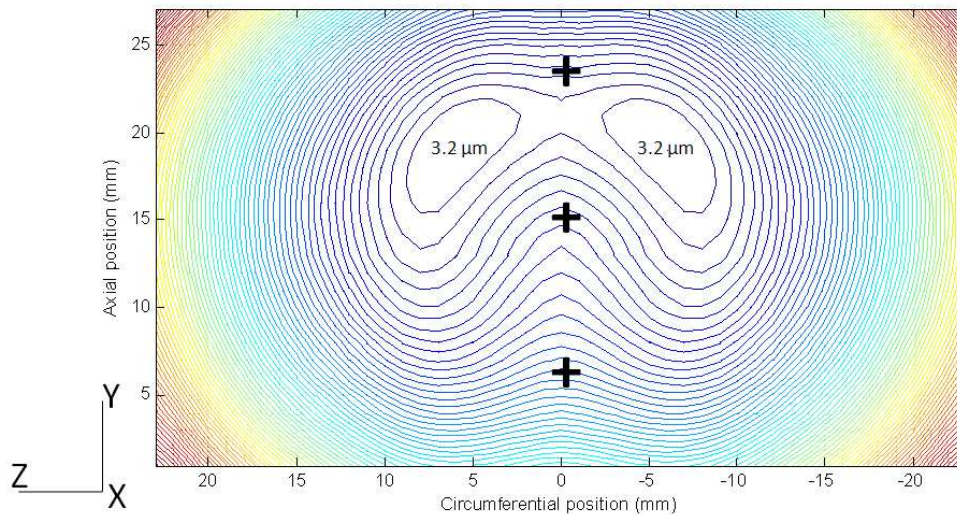
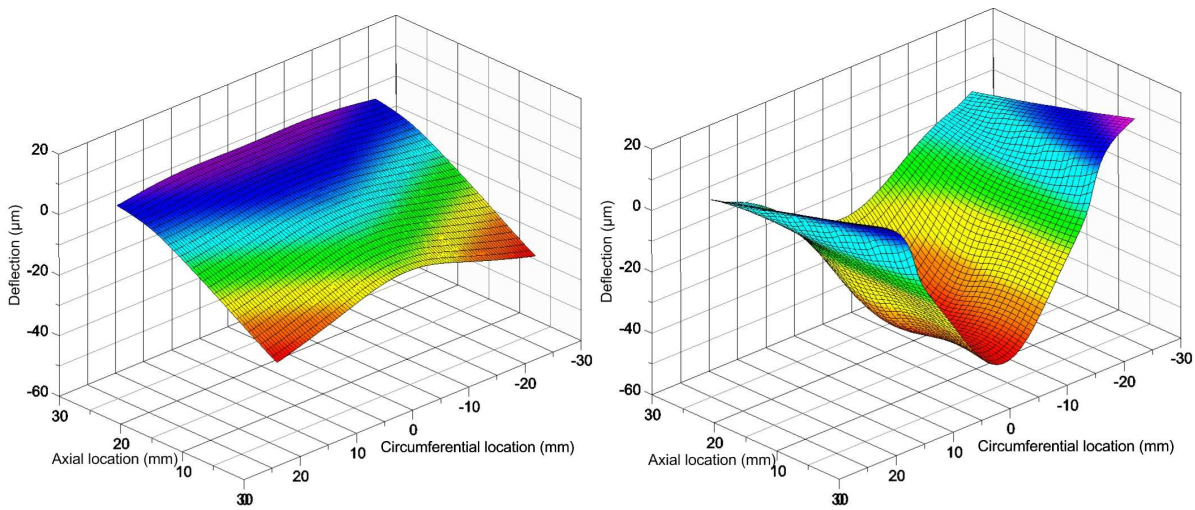


**Figure 7: Lubricant Film thickness contour and marked measurement positions**

The film thickness contour of figure 7 shows a significant deviation from the original barrel profile of an undeformed film thickness shape. The two major component parts of the distortion originate from the in-cylinder pressure acting upon the piston crown and the load normal to the surface of the skirt, generated by lubricant and boundary pressures. Although included in the calculations, the inertial-induced piston distortion is two orders of magnitude smaller (thus not shown). The two aforementioned dominant contributions are shown in figures 9(a) and 9(b).



(a)- Radial deformation due to piston crown pressure loading      (b)- Radial deformation due to normal loadings

**Figure 8: Components of piston skirt deformation**

The largest deflections originate from the normal loads and induce maximum deflections at the centre of the skirt towards its bottom edge. This is because of the design of the skirt with preferential stiffness at its top edge. In effect, the skirt acts like a cantilever with its least structural stiffness at its lower edge. Radial deflections of up to  $50\mu\text{m}$  are typical under these conditions, because of the relatively low bulk and sectional modulus of the piston skirt. The bending action due to the cylinder pressure loading tends to move the minimum film thickness position towards the crown. This response mode is seen clearly in figure 8(a). This effect also acts to increase the entraining wedge of the skirt when the piston undergoes the combustion stroke and is subjected to the most significant cylinder pressures. These two effects combine significantly to reduce the load carrying contribution of the bottom of the skirt under aligned piston operation, but improve the hydrodynamic wedge effect, thus increasing the film thickness and reduce friction.

Balakrishnan [29] did not account for the thermo-elastic deformation of the piston and skirt. He drew comparisons between the semi-infinite solid nature of localised skirt deformation using the time consuming effective influence Newton (EIN) method [30,31] and the simpler column method [6,32] based on the prevailing soft-type elastohydrodynamic conditions, showing a deviation of merely 5% between them. He, therefore, opted for the latter approach for rapid computational convergence. The current paper shows that although the main component of radial deformation is due to conjunctural pressures, significant thermo-elastic deformation also occurs as the result of in-cylinder pressure. Balakrishnan's approach does not take this contribution into account. An *effective* stiffness matrix was previously used by Littlefair *et al* [33] which evaluated the nodal distortion of a point only from its direct normal force in the same manner as the column method approach, but using an FEM model. Thus a specific nodal response was calculated for a true 3D model, rather than a uniform nodal response using a column method approach. For the case detailed here the converged pressure distribution was applied to the effective stiffness matrix created in the same manner. Figure 9 shows comparison of calculated deflections from normal loads with different methods along the centre line of the skirt in the axial direction of the piston. This direct comparison shows the significant effect of a nodal pressure on the surface as a whole, rather than just at the point of application. The development of the compliance method here is critical to the calculation of the 3D distortion shape within a timescale that is not detrimental to iterative procedures.

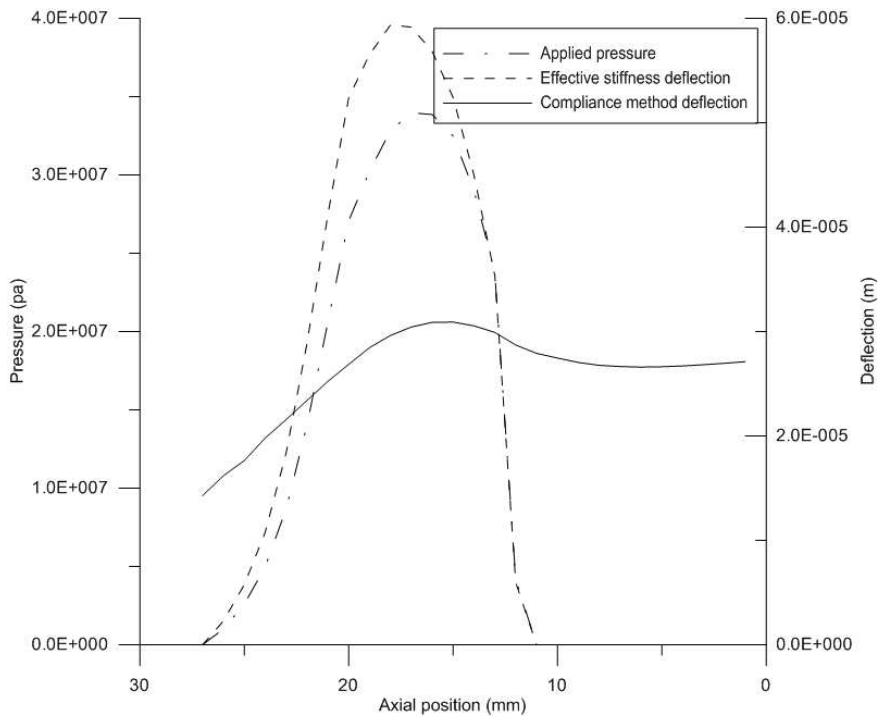


**Figure 9: Comparison of normal distortion techniques**

The smaller skirt deflection reported in [10] results in pressure spikes at the relief radii of the piston skirt profile at its extremities and lower pressures in the contact domain (figure 10(a)). The pressure distribution in figure 11(b), in the current analysis, on the other hand shows a different contact patch mainly owing to more accurate evaluation of deformed skirt profile as well as the use of a compliant skirt structure.

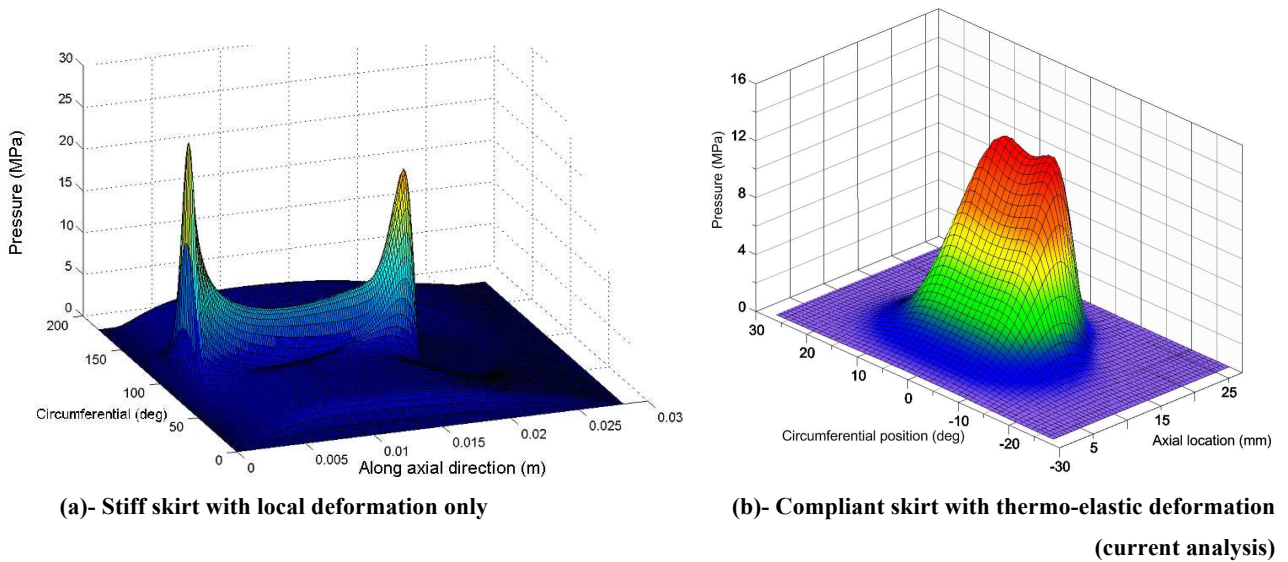


**Figure 10: Piston skirt-liner pressure distribution**

## 5. Conclusions

The paper has described measurement and prediction of lubricant film thickness in piston skirt-cylinder liner conjunction. The study shows good agreement between predictions and measurements. It further highlights the importance of accurate prediction of skirt deformation due to generated conjunctural pressures as well as global thermo-elastic deformation of piston and skirt structures subjected to in-cylinder pressures and temperatures. The global deformation is particularly important in light weight pistons with fairly compliant skirt structures. These are the attributes of high performance race engines, a trend which is set to become commonplace for most future engines.

## 6. Acknowledgements:

The authors wish to express their gratitude to the EPSRC for the financial support extended to the Encyclopaedic Program Grant, under which this research was carried out. Thanks are also due to the consortium of industrial partners of the Encyclopaedic project, particularly in this instance Capricorn Automotive.

## 7. References

- [1]- Fitzsimons, B., "Introduction to the importance of fuel efficiency and role of the Encyclopaedic research project", *IMEchE Seminar on A Drive for fuel efficiency, Loughborough, 2011*
- [2]- Knoll, G. D. and Peecken, H. J., "Hydrodynamic lubrication of piston skirts", *Trans. ASME, J. Lubn. Tech.*, 104, 1982, pp. 504–509
- [3]- Balakrishnan, S. and Rahnejat, H., "Isothermal transient analysis of piston skirt-to-cylinder wall contacts under combined axial, lateral and tilting motion", *J. Phys., D: Appl. Phys.*, 38(5), 2005, 787
- [4]- Kushwaha, M. and Rahnejat, H., "Transient elastohydrodynamic lubrication of finite line conjunction of cam to follower concentrated contact", *J. Phys., D: Appl. Phys.*, 35(21), 2002, 2872
- [5]- Sadeghi, F., "Elastohydrodynamic Lubrication", in *Rahnejat (Ed.), Tribology and Dynamics of Engine and Powertrain: Fundamentals, Applications and Future Trends*, Woodhead Publishing, Cambridge, 2010, ISBN-10: 1845693612
- [6]- Gohar, R. and Rahnejat, H., *Fundamentals of Tribology*, Imperial College Press, London, 2008, ISBN-10: 1848161840
- [7]- Perera, M.S.M., Theodossiades, S. and Rahnejat, H., "Elasto-multi-body dynamics of internal combustion engines with tribological conjunctions", *Proc. IMechE, Part K: J. Multi-body Dyn.*, 224(3), 2010, pp. 261-277
- [8]- Dursunkaya, Z. and Keribar, R., "Simulation of secondary dynamics of articulated and conventional piston assemblies", *SAE Paper No. 920484*, 1992
- [9]- Offner, G. and Priebsch, H. H., "Elastic body contact simulation for predicting piston slap induced noise in an IC engine", in *Rahnejat, H., Ebrahimi, M. and Whalley, R. (Eds.), Multi-body dynamics: Monitoring and simulation techniques – II*, Professional Engineering Publishing (IMEchE), ISBN 1-86058-258-3 p191-206
- [10]- Balakrishnan, S., Howell-Smith, S. and Rahnejat, H., "Investigation of reciprocating conformal contact of piston skirt-to-surface modified cylinder liner in high performance engines", *Proc. IMechE, Part C: J. Mech. Engng. Sci.*, 219(11), 2005, pp. 1235–1247
- [11]- Hoshikawa, J., Kiminari, K., Miyamoto, K. and Higashi, H., "A study of friction reduction by 'Soft Skirt' Piston". *SAE pap. No. 2011-01-2120*, 2011
- [12]- Bai, D., Modeling piston skirt lubrication in internal combustion engines, PhD Thesis, Massachusetts Institute of Technology, USA, 2012
- [13]- McClure, F., Numerical modeling of piston secondary motion and skirt lubrication in internal combustion engines, PhD thesis, Massachusetts Institute of Technology, USA, 2007
- [14]- Howell-Smith, S.J., Tribological optimisation of the internal combustion engine piston to bore conjunction through surface modification, PhD Thesis, Loughborough University, 2011
- [15]- Rahnejat, H., *Multi-body Dynamics: Vehicles, Machines and Mechanisms*, PEP (IMEchE) and SAE, 1998, ISBN 0-7680-0269-9
- [16]- Dwyer-Joyce, R.S., Green, D.A., Balakrishnan, S., Harper, P., Lewis, R., Howell-Smith, S.J, King, P.D. and Rahnejat, H., "The measurement of liner-piston skirt oil film thickness by an ultrasonic means", *SAE Tech. Pap. No. 2006-01-0648*, 2006
- [17]- Avan, E.Y., Mills, R. and Dwyer-Joyce, R., "Ultrasonic Imaging of the piston ring oil film during operation in a motored engine – Towards oil film thickness measurement", *SAE pap No. 2010-01-2179*, 2010

- [18]- Mills, R.S., Avan, E.Y. and Dwyer-Joyce, R.S. "Piezoelectric sensors to monitor lubricant film thickness at piston-cylinder contacts in a fired engine". *Proc. IMechE Part J: J. Engng. Trib.*, 227(2), 2012, pp.100-111
- [19]- Shin, S., Cusenza, A., and Shi, F., "Offset crankshaft effects on SI engine combustion and friction Performance," *SAE Technical Paper 2004-01-0606*, 2004, doi:10.4271/2004-01-0606
- [20]- Roelands C. J. A., "Correlation Aspects of the viscosity-Temperature-Pressure Relationships of Lubricating Oils", *Druk VRB Kleine der A3-4 Groningen*, 1966
- [21]- Dowson, D. and Higginson, G.R., "A numerical solution to the elastohydrodynamic problem", *J. Mech. Engng. Sci.*, 6(1), 1959
- [22]- Greenwood, J. A. and Tripp, J. H., "The contact of two nominally flat rough surfaces", *Proc. IMechE., J. Mech. Engng. Sci.*, 185, 1970-71, pp.625-633
- [23]- Hu Y, Cheng HS, Arai, T., et al., "Numerical simulation of piston ring in mixed lubrication – A non-axisymmetrical Analysis", *Trans ASME, J. Trib.*, 116, 1994, pp. 470–478.
- [24]- Teodorescu, M., Balakrishnan, S. and Rahnejat, H., "Integrated tribological analysis within a multi-physics approach to system dynamics", *Tribology and Interface Engineering Series, Elsevier*, 48, 2005, pp. 725-737
- [25]- D'Agostino, V., Guida, D., Ruggiero, A. and Russo, C., "Optimised EHL Piston Dynamics computer code", *AITC-AIT, Int. Conf. on Tribology, 20-22 Sept 2006 Parma, Italy*
- [26]- Ning, L., Meng, X. and Xie, Y., "Incorporation of deformation in a lubrication analysis for automotive piston skirt–liner system", *Proc. IMechE, Part J: J. Engng. Trib.*, Nov 30th 2012 doi: 10.1177/1350650112466768, Published online.
- [27]- Dias da Cunha, R. and Hopkins, T., "PIM 1.1 — the parallel iterative method package for systems of linear equations user's guide — Fortran 77 version Technical Report Computing Laboratory", University of Kent at Canterbury, Kent, UK, 1994.
- [28]- Bosch, *Automotive Handbook*, 7th Edition, John Wiley and Sons, 2007
- [29]- Balakrishnan, S., Transient elastohydrodynamic analysis of piston skirt lubricated contact under combined axial, lateral and tilting motion, *PhD Thesis, Loughborough University, UK, 2002*
- [30]- Ehret, P., Dowson, D., Taylor, C.M. and Wang, D., "Analysis of isothermal elastohydrodynamic point contacts lubricated by Newtonian fluids using multigrid methods", *Proc. IMechE, Part C: J. Mech. Engng. Sci.*, 211(7), 1997, pp. 493-508
- [31]- Jalali-Vahid, D., Rahnejat, H., Jin, Z.M. and Dowson, D., "Transient analysis of isothermal elastohydrodynamic circular point contacts", *Proc. IMechE, J. Mech. Engng. Sci., Part C: 215(10)*, 2001, pp. 1159-1172
- [32]- Rahnejat, H., "Multi-body dynamics: historical evolution and application", *Proc. IMechE, Part K: J. Multi-body Dyn.*, 214(1), 2000, pp. 149-173
- [33]- Littlefair, B., Howell-Smith, S., Rahnejat, H. and Theodossiades, S., "Assessment of thermo-structural effects on EHL piston skirt lubrication", *Proceeding of ASME 2012 Internal Combustion Engine Division Spring Technical Conference*, 6-9 May 2012, ICES2012-81125

## Nomenclature

### Latin characters

$A$  - Condensed pre-calculated piston response [-]  
 $A_c$  - Apparent contact area [ $m^2$ ]  
 $c$  - Nominal clearance [ $m$ ]  
 $c_s$  - Speed of sound in the lubricant [ $m.s^{-1}$ ]  
 $C_p$  - Crank offset [ $m$ ]  
 $E'$  - Equivalent (reduced) modulus of elasticity [ $Pa$ ]  
 $F$  - Force array [ $N$ ]  
 $F_s$  - Skirt side force [ $N$ ]  
 $F_2, F_{5/2}$  - Statistical functions [-]  
 $h$  - Film thickness [ $m$ ]  
 $i, j, k, l$  - Array position indicators [-]  
 $it$  - Iteration number [-]  
 $K$  - Stiffness array [ $N/m$ ]  
 $l$  - Connecting rod length [ $m$ ]  
 $L_u$  - Localised normal reference loading [ $N$ ]  
 $m$  - Spatial deflection index [-]  
 $m_g$  - Gudgeon mass [ $kg$ ]  
 $m_p$  - Piston mass [ $kg$ ]  
 $nyy$  - Number of nodes in y-direction [-]  
 $nzz$  - Number of nodes in z-direction [-]  
 $p$  - Pressure [ $Pa$ ]  
 $P_b$  - Boundary pressure [ $Pa$ ]  
 $P_{cy}$  - Cylinder pressure [ $Pa$ ]  
 $P_{ref}$  - Reference pressure loading [ $Pa$ ]  
 $P_v$  - Viscous pressure [ $Pa$ ]  
 $r$  - Crankshaft Radius [ $m$ ]  
 $r_p$  - Piston radius [ $m$ ]  
 $R$  - Acoustic reflection coefficient [-]

$S_{i,j}$  - starting skirt shape [ $m$ ]  
 $t$  - Time [ $s$ ]  
 $u_{av}$  - Average body speed in y direction [ $m.s^{-1}$ ]  
 $v_{av}$  - Average body speed in z direction [ $m.s^{-1}$ ]  
 $W$  - Reference load [ $N$ ]  
 $W_a$  - Load carried by asperity contact [ $N$ ]  
 $x, y, z$  - Cartesian coordinates  
 $y_p$  - Piston displacement from TDC [ $m$ ]  
 $\dot{y}_p$  - Primary piston velocity [ $m.s^{-1}$ ]  
 $\ddot{y}_p$  - Primary piston acceleration [ $m.s^{-2}$ ]  
 $\ddot{y}_m$  - Reference piston acceleration negative [ $m.s^{-2}$ ]  
 $\ddot{y}_p$  - Reference piston acceleration positive [ $m.s^{-2}$ ]  
 $Z$  - Acoustic impedance of the skirt and liner materials [ $N.s.m^{-3}$ ]

### Greek characters

$\beta$  - Fitting co-efficient [-]  
 $\delta SI$  - Skirt deflection from normal loading [ $m$ ]  
 $\delta$  - Skirt overall deflection [ $m$ ]  
 $\delta Cp$  - Skirt deflection from Crown loading [ $m$ ]  
 $\delta In$  - Skirt deflection from inertial loading [ $m$ ]  
 $\varepsilon_L$  - Load convergence tolerance [ $N$ ]  
 $\varepsilon$  - Crown loading shape response [ $m$ ]  
 $\varepsilon ip$  - Primary inertial loading shape response, positive direction [ $m$ ]  
 $\varepsilon in$  - Primary inertial loading shape response, negative direction [ $m$ ]  
 $\varepsilon_{rp}$  - Pressure convergence tolerance [-]  
 $\vartheta_p$  - Pressure relaxation coefficient [-]  
 $\theta$  - Crankshaft angle [ $^\circ$ ]

$\xi$  - Number of asperities per unit contact area

[ $m^{-2}$ ]

$\eta$  - Effective viscosity in conjunction [ $Pa.s$ ]

$\eta_o$  - Viscosity at inlet [ $Pa.s$ ]

$\bar{\eta}$  - Pressure corrected viscosity [-]

$\kappa$  - Average asperity tip radius [ $m$ ]

$\lambda$  - Stribeck's oil film parameter [-]

$\rho$  - Effective lubricant density [ $kg.m^{-3}$ ]

$\rho_o$  - Inlet lubricant density [ $kg.m^{-3}$ ]

$\sigma$  - rms of roughness of contiguous surfaces [ $m$ ]

$\phi$  - Connecting-rod angle [ $^{\circ}$ ]

$\omega$  - Crank rotational velocity [ $rad.s^{-1}$ ]

$\Omega$  - Clearance relaxation coefficient [-]